Theoretical Study on the Mechanism and Thermodynamic of Methanethiol and Ozone Reaction

ARTICLE *in* COMPUTATIONAL AND THEORETICAL CHEMISTRY · AUGUST 2014

Impact Factor: 1.55 · DOI: 10.1016/j.comptc.2014.04.028

3 AUTHORS, INCLUDING:

Morteza Vahedpour

University of Zanjan

45 PUBLICATIONS **185** CITATIONS

Computational and Theoretical Chemistry 1042 (2014) 41–48

Contents lists available at ScienceDirect

Computational and Theoretical Chemistry

journal homepage: www.elsevier.com/locate/comptc

Theoretical study on the mechanism and thermodynamic of methanethiol and ozone reaction

Morteza Vahedpour *, Fereshte Karami, Javad Shirazi

Department of Chemistry, University of Zanjan, P.O. Box 45371-38791, Zanjan, Iran

ARTICLE INFO

Article history:
Received 12 November 2013
Received in revised form 27 April 2014
Accepted 27 April 2014
Available online 20 May 2014

Keywords:
Methanethiol
Oxidation
Theoretical calculation
Reaction pathway

ABSTRACT

Reaction mechanism of methanethiol oxidation with ozone are carried out using the B3LYP and CCSD(T) theoretical approaches in connection with the 6-311++G(3df,3pd) basis set. Results confirm six kinds of products, P1–P6, which have enough thermodynamic stability. In thermodynamic viewpoint, the P6 product is the most favored adduct of the $CH_3SH + O_3$ gas phase reaction at atmospheric pressure and 298.15 K temperature. The P6 adduct, $CH_3OH + SO_2$, is spontaneous and exothermic with −146.47 and −146.81 kcal/mol in Gibbs free energy and enthalpy of reaction at the B3LYP level, respectively. In kinetic viewpoint, the $CH_2S + H_2O_2 + O_2$, P2 adduct, as final product after passing two transition state low level is the most favorite path.

1. Introduction

Organic sulfide compounds play an important role in tropospheric chemistry. Thiols are highly reactive sulfur-containing species well known for their disagreeable odors. The most volatile of thiols is methanethiol (also known as methyl mercaptan), which is one of the natural sources of sulfur compounds emitted into the atmosphere. Due to the extremely low odor threshold of methanethiol, it is added to natural gas, enabling people to detect leaks by smell. Methanethiol is the most simple and important atmospheric sulfide which is commonly known to cause serious environmental and human health problems [1]. It is also a colorless weak acid, found in the blood and brain of humans and other animal as well as planet tissues. At very high concentration it is highly toxic and affects the central nervous system [2].

Methanethiol (CH_3SH) is one of the most important products of degradation of organic matter, it is released from decaying organic matter in marshes and it is present in coal tar and some crude oils [3]. In addition, colonic bacteria produce large quantities of the highly methanethiol [4].

In anoxic freshwater sediments dimethyl sulfide and methanethiol are generally considered to be the dominant volatile organic sulfur compounds. Fluxes of methanethiol from freshwater systems toward the atmosphere depend on the steady-state concentration of the balance between its formation and degradations. It is used as an additive and odorant in the light hydrocarbon streams such as refinery gas and in fuels including natural gas in the United States and Europe. Methyl mercaptan is one of the natural sources of sulfur emitted into the atmosphere. So, the process of removal of methane thiol is of great scientific and practical importance [1].

CH_3OH–H_2S route for the synthesis of methanethiol is an inefficient process, which proceeds via a methane steam reforming to syngas ($CO + H_2$) and the synthesis of methanol from syngas. Methanethiol, CH_3SH, is very active and can be used an important intermediate in the production of organosulfur compounds, pesticide, medicine and synthetic material [5]. However, it is mainly used to produce methionine, which use as a dietary component in poultry and animal feed. Methanethiol is also used in the plastics industry and as a precursor in the manufacture of pesticides.

Oxidation reactions of organic sulfides are of great importance in biological systems [6,7], both in the atmosphere [8] and on surfaces [9]. The gas phase oxidation of organic sulfur compounds has become of increasing importance in relation with pollution by SO_2 and tropospheric and stratospheric sulfur containing aerosols [10] methanethiol is interesting in view of its presence in the Earth's atmosphere. It can further be used as an important intermediate in the production of organosulfur compounds, such as dimethyl sulfoxide, and dimethyl sulfone [11].

The oxidation of CH_3SH ultimately leads to the formation of SO_2 and results in the formation and growth of sulfate aerosols, which are the main sources of cloud-condensation nuclei, removed by highly acidic precipitation [12]. CH_3SH has been removed from the stream by catalytic incineration [13], chemisorptions [14], and packed tower scrubbing [15].

* Corresponding author. Tel.: +98 24 33052631; fax: +98 24 33052477.
E-mail address: vahed@znu.ac.ir (M. Vahedpour).

http://dx.doi.org/10.1016/j.comptc.2014.04.028
2210-271X/

So far, related experimental and theoretical studies with the present study, such as on CH_3SH with OH, HO_2, NO_3, and Cl reactions have been done in the gas phase. Particularly, the reaction of CH_3SH with OH has been the subject of numerous kinetic studies. Atkinson et al. studied the $CH_3SH + OH$ reaction in argon by the flash photolysis technique at 50–100 Torr, and obtained an Arrhenius expression of $k = 8.89 \times 10^{-12} \exp[(398 + 151)/T]$ cm^3 molecule^{-1} s^{-1} [16]. Wine et al. used very similar conditions and the same technique, that obtained the expression $k = 1.15 \times 10^{-11} \exp[(338 + 100)/T]$ cm^3 molecule^{-1} s^{-1} [17]. In later studies, Wine and co-workers attempted to elucidate mechanistic details of the reaction [18,19]. Another competitive rate study by Barnes et al. produced a rate constant of $k_{298} = (3.6 + 0.4) \times 10^{-11}$ cm^3 molecule^{-1} s^{-1}, in agreement with the flash photolysis studies [20]. Based upon a least-squares analysis of the absolute rate coefficients of Atkinson et al. [16], Wine et al. [17,19] and Hynes and Wine [18] become $k = 3.3 \times 10^{-11}$ cm^3 molecule^{-1} s^{-1} at 298 K. In studies of $HO_2 + CH_3SH \rightarrow$ products reaction, Mellouki and Ravishankara has shown that the absolute rate coefficient is $k < 4 \times 10^{-15}$ cm^3 molecule^{-1} s^{-1} at 298 K [21]. Wallington et al. obtained $k = (8.1 + 0.6) \times 10^{-13}$ cm^3 molecule^{-1} s^{-1} for $NO_3 + CH_3SH$ reaction [22].

The sulfur atom can bind to one or more oxygen and hydrogen atoms, or hydrogen atoms can absorbed with oxygen atoms of the ozone molecules, and carbon can bind to oxygen atom instead of sulfur.

Ozone is an important constituent of the atmosphere; its main role is preventing UV rays reaching the Earth's surface. The reaction of this material with gaseous compounds is of high importance. The $CH_3SH + O_3$ reaction mechanism has been studied in this letter by means of computational methods based on quantum theory, characterizing all the minima and transition states on all pathways. The results obtained have allowed us to compare the likelihood of each way in order to determine which reaction pathway is energetically and kinetically favored.

In spite of slow reaction rates, the thermodynamic stability of products such as SO_2 and methanol, and the atmospheric importance of adducts are our motivation for doing this investigation. So, the aim of the present work is analysis of the thermodynamic and kinetic aspects of the methanethiol and ozone oxidation reactions. The gas phase reaction are investigated and suggested the mechanism for formation of six possible products as $CH_3SHO + {}^3O_2$, $CH_2S + H_2O + {}^3O_2$, $CH_2SHOH + {}^3O_2$, $HCOSH + H_2O_2$, $CH_2SO_2 + H_2O$ and $CH_3OH + SO_2$. Some of these products are produced from one reaction path, but some derive from two or more paths.

2. Computational method

All the calculations are performed with the Gaussian 03 program [23]. In the first step all the geometry optimizations were carried out using density functional theory (DFT) B3LYP [24] with the 6-311++G(3df-3pd) basis set [25]. All the obtained total energies were corrected with the zero point energy. To compute accurate relative energies, calculations are carried out at the CCSD(T) [26] method. In the above calculations, we report the T1 diagnostic values, which give a qualitative assessment of the significance of nondynamical correlation [27]. In order to obtain the total energies, the CCSD(T) energies are corrected with the zero point vibrational energy estimated by B3LYP/6-311++G(3df,3pd) calculations. The CCSD(T) have been employed for refining the electronic energies of the optimized structures. Total and relative energies of all species in the reaction were derived from B3LYP and CCSD(T) levels. Connection between reactants, intermediates, transition states, and products are confirmed by the intrinsic reaction coordinate (IRC) [27,28] method. The IRC method has been used to describe minimum energy paths from transition state structures to the corresponding minima at the B3LYP level. Thermodynamic data for reactions are calculated at the B3LYP level. We computed the vibrational frequencies for the verification of the optimized geometries. Any reactant, product, and intermediate possess all real frequencies and all transition states have exactly one imaginary frequency. In addition, to confirm the optimized structures of all species and their atomic connectivity, the topological analyses of atoms in molecules (AIM) [29] were carried out by means of the AIM 2000 series of programs [30]. All these calculations are done at a temperature of 298.15 K and under atmospheric pressure.

3. Results and discussion

All the elementary reactions of methanethiol and ozone begins with the formation of a quasi-bound complex (C1–C4), followed by formation of a transition state (TS1–TS9) and some intermediates (IN1–IN7). In the exit channels, complex formation does also occur before the reaction products are formed these are labeled CP1–CP6. The optimized geometries for the $CH_3SH + O_3$ reaction at the B3LYP level are shown in Fig. 1. In Table 1, the total energies are given for the B3LYP and CCSD(T) levels and corresponding relative energies in comparison with the original reactants. In addition, T1 diagnostic in the CCSD(T) of all species are tabulated in Table 1. In this work, the stabilization energy is defined as the energy difference between the pre-reactive complex and the reactants. The energy difference between the transition state structure and the pre-reactive complex is denoted as the activation barrier. The reaction energy is the energy difference between the products and the reactants. To simplify our discussion, the energy of reactants, R ($CH_3SH + O_3$), is set to be zero for reference. Figs. 2 and 3 schematically display the energetic profiles for $CH_3SH + O_3$ reaction at the CCSD(T) level. Fig. 2, shows the reaction pathways for production of P1–P4 and Fig. 3 schematize the reaction pathways for the P5–P6 products. The calculated vibrational frequencies at the B3LYP level are listed in Table 1S in Supplementary data. All intermediate, INs, and pre-reactive complex, Cs, are true minima on the reaction PES and transition state, TS, has only one imaginary frequency. Table 2 gives the reaction internal energies, enthalpies, Gibbs free energies, and entropies at room temperature. The overall rate constant (in cm^3 molecule^{-1} s^{-1}) for P2 in the temperature range of 200–1000 K at the B3LYP/6-311++G(3df,3pd) has been calculated in Table 3. Finally, Fig. 4 shows an Arrhenius curves for the reaction rate constant k_T for P2 production of $CH_3SH + O_3$ reaction.

3.1. Reactants and initial complex formations

Four pre-reactive complexes are found when the original reactants approach to each other as C1, C2, C3 and C4. Pre-reactive complex C1 is formed when the terminal oxygen atom of molecular ozone approaches to the H4 hydrogen atom of methanethiol and the central oxygen atom of O_3 reacts with the sulfur atom of methanethiol. The interaction of H4 of methanethiol with a lone pair of terminal oxygen atom of O_3 in one side and interaction of O2 atom with a lone pair of sulfur atom of methanethiol in other side, leads to the formation of a five-membered ring complex, which named C1. The newly bonds formation in C1, H4–O3 and S8–O2, lengths are 2.391, and 3.310 Å, respectively. Hence, one of newly bonds formation (H4–O3) in C1 is a hydrogen bond. The bond length of O2–O3 in C1 is 1.257 Å longer than the corresponding bond in ozone, which corresponds to a relative increase of 5% at the B3LYP level. The formations of newly bonds are confirmed by an AIM topological analysis of wave function. This analysis reveals the presence of bond critical points (bcp), located between S8 and

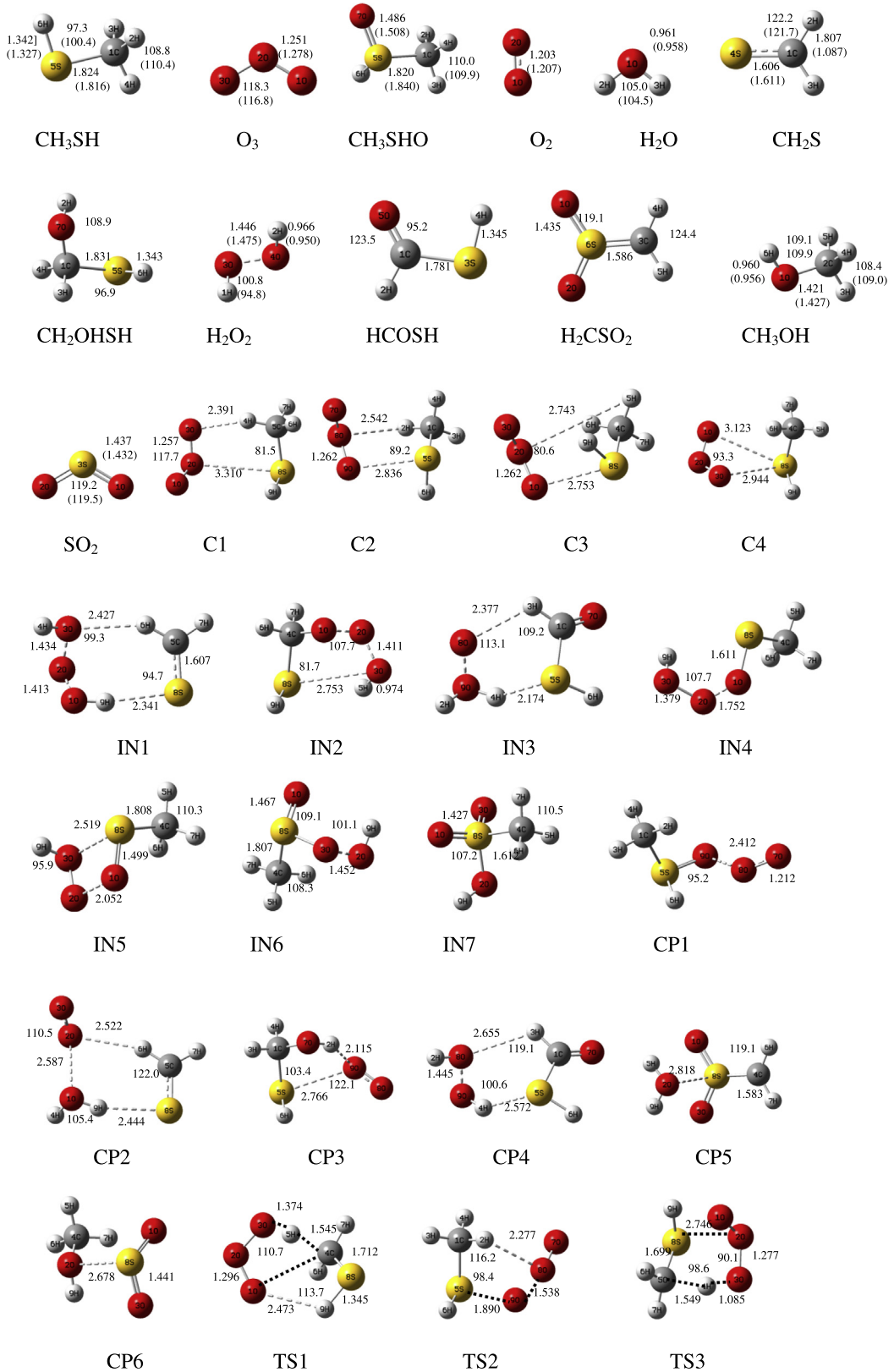

Fig. 1. Geometries of reactants, products, intermediates and transition states optimized at the B3LYP level (bond distances are in angstrom and angles are in degree). The values in square parentheses refer to experimental data [37,38].

O2 [ρ (r_{bcp}) = 0.0078 au and $\nabla^2\rho$ (r_{bcp}) = 0.0226 au] and the presence of the bcp located between H4 and O3 [ρ (r_{bcp}) = 0.0104 au and $\nabla^2\rho$ (r_{bcp}) = 0.0349 au]. The sign and values of the electronic charge density and its Laplacian are characteristic of hydrogen bond formation between H4 and O3 and the S8–O2 interaction as being of the van der Waals type. The formation of C1 is barrier-less process with a stabilization energy of 1.79 kcal/mol with respect to the reactants at the CCSD(T) level.

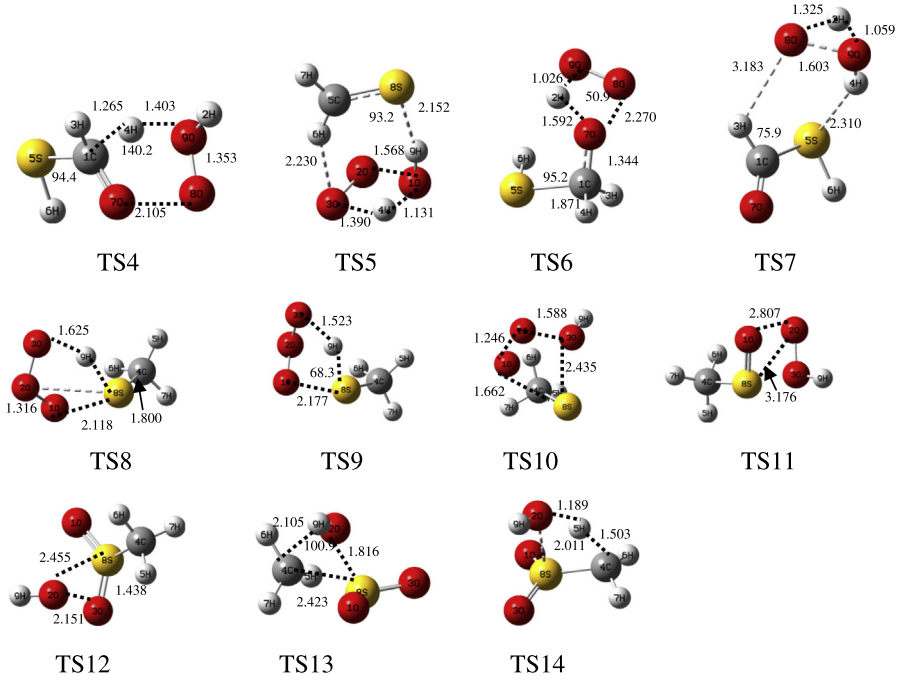

Fig. 1 (*continued*)

Table 1
The total energies (in Hartree) and relative energies (in kcal/mol) of the reactants, products and intermediates, and T1 diagnostic in the $CH_3SH + O_3$ reaction.

Species	B3LYP	CCSD(T)	T1 diagnostic
R($CH_3SH + O_3$)	−664.1983(0)	−663.2446(0)	–
C1	−664.1993(−0.596)	−663.2475(−1.791)	0.021
C2	−664.2004(−1.308)	−663.2456(−0.599)	0.021
C3	−664.2008(−1.543)	−663.2450(−0.284)	0.022
C4	−664.2022(−2.420)	−663.2479(−2.066)	0.021
IN1	−664.2482 (−31.270)	−663.3158(−44.696)	0.016
IN2	−664.2685(−44.040)	−663.3145(−43.843)	0.016
IN3	−664.2923(−58.972)	−663.3353(−56.923)	0.019
IN4	−664.2612(−39.446)	−663.3010(−35.401)	0.021
IN5	−664.2687(−44.136)	−663.3129(−42.855)	0.021
IN6	−664.3348(−85.627)	−663.3782(−83.814)	0.018
IN7	−664.4418(−152.789)	−663.4921(−155.273)	0.016
TS1	−664.1689(18.484)	−663.2240(12.946)	0.072
TS2	−664.1718(16.668)	−663.2103(21.549)	0.065
TS3	−664.1724(16.263)	−663.2230(13.596)	0.065
TS4	−664.2155(−10.783)	−663.1759(43.124)	0.024
TS5	−664.1831(9.580)	−663.2291(9.719)	0.023
TS6	−664.2037(−3.391)	−663.2644(−12.409)	0.053
TS7	−664.2805(−51.573)	−663.3263(−51.245)	0.023
TS8	−664.1909(4.635)	−663.2304(8.953)	0.043
TS9	−664.1914(4.324)	−663.2322(7.785)	0.046
TS10	−664.1706(17.382)	−663.2433(0.783)	0.098
TS11	−664.2657(−42.285)	−663.3051(−37.920)	0.042
TS12	−664.2929(−59.341)	−663.3471(−64.321)	0.051
TS13	−664.3280(−81.383)	−663.3651(−75.597)	0.032
TS14	−664.3458(−92.535)	−663.3907(−91.632)	0.017
CP1	−664.2347(−22.810)	−663.2824(−23.711)	0.017
CP2	−664.2496(−32.142)	−663.3049(−37.841)	0.016
CP3	−664.2680(−43.710)	−663.3175(−45.722)	0.015
CP4	−664.3555(−98.598)	−663.4005(−97.838)	0.015
CP5	−664.3930(−122.158)	−663.4407(−123.031)	0.016
CP6	−664.4375(−150.079)	−663.4836(−149.931)	0.017
^{1}P1($CH_3SHO + {}^1O_2$)	−664.1508(−20.360)	−663.2794(−21.836)	–
^{3}P1($CH_3SHO + {}^3O_2$)	−664.2921(−58.830)	−663.3276(−52.082)	–
^{1}P2($CH_2S + H_2O + {}^1O_2$)	−664.2446(−29.023)	−663.2980(−33.463)	–
^{3}P2($CH_2S + H_2O + {}^3O_2$)	−664.3059(−67.493)	−663.3462(−63.710)	–
^{1}P3($CH_2SHOH + {}^1O_2$)	−664.2635(−40.903)	−663.3172(−45.528)	–
^{3}P3($CH_2SHOH + {}^3O_2$)	−664.3248(−79.373)	−663.3654(−75.775)	–
P4($CHOSH + H_2O_2$)	−664.3530(−97.032)	−663.3946(−94.118)	–
P5($CH_2SO_2 + H_2O$)	−664.3893(−119.857)	−663.4341(−118.906)	–
P6($CH_3OH + SO_2$)	−664.4322(−146.721)	−663.4607(−135.569)	–

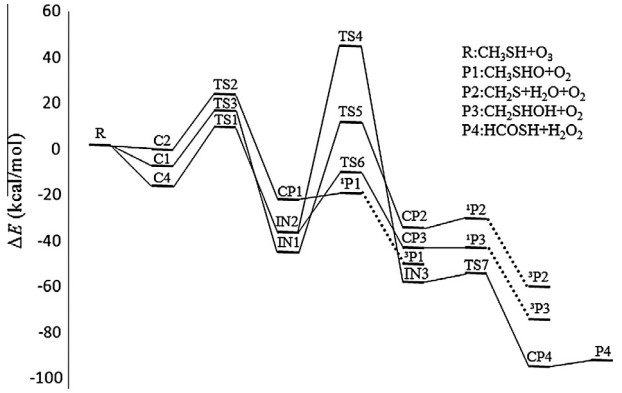

Fig. 2. A schematic energy profile along the arbitrary reaction coordinates. The stationary points of the reaction between the methanethiol and ozone with the final product of P1–P4 at the CCSD(T) method.

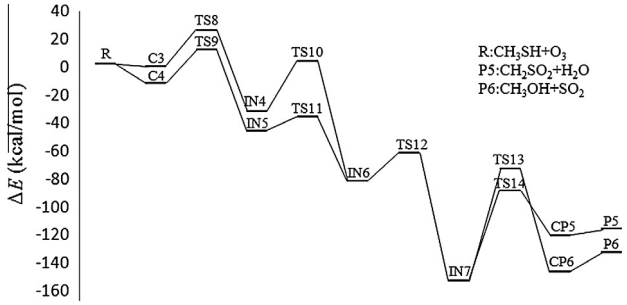

Fig. 3. A schematic energy profile along the arbitrary reaction coordinates. The stationary points of the reaction between the methanethiol and ozone with the final product of P5–P6 at the CCSD(T) method.

Table 2
The thermodynamic data for $CH_3SH + O_3$ reaction at the B3LYP method (kcal/mol).

Reaction	ΔE^0	ΔH^0	ΔG^0	$T\Delta S^0$
$CH_3SH + O_3 \rightarrow CH_3SHO + {}^3O_2$	−58.886	−58.887	−57.623	−1.264
$CH_3SH + O_3 \rightarrow CH_2S + H_2O + {}^3O_2$	−66.515	−65.923	−75.793	9.869
$CH_3SH + O_3 \rightarrow CH_2OHSH + {}^3O_2$	−79.319	−79.319	−78.278	−1.041
$CH_3SH + O_3 \rightarrow CHOSH + H_2O_2$	−96.870	−96.870	−96.859	−0.012
$CH_3SH + O_3 \rightarrow CH_2SO_2 + H_2O$	−119.635	−119.636	−117.991	−1.645
$CH_3SH + O_3 \rightarrow CH_3OH + SO_2$	−146.806	−146.806	−146.475	−0.331

The second pre-reactive complex, C2, has a five-membered-ring structure. This structure is composed from two simultaneous interactions of involved atoms between methanethiol and ozone molecules. One interaction is between H4 atom of methanethiol with a lone pair of the terminal O2 atom of molecular O_3. The H4–O2 bond length is calculated 2.542 Å. Another interaction between O1 of molecular ozone with the S8 of methanethiol is formed O1–S8 bond with the length of 2.836 Å. The formation of newly

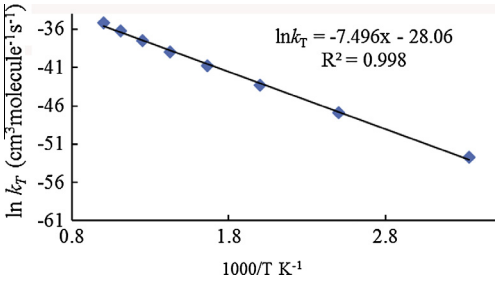

Fig. 4. Arrhenius curves for the reaction rate constant k_T for P2 of $CH_3SH + O_3$ reaction.

bonds are confirmed by the topological analysis of the wave function that reveals the existence of two bcp, one located between H4 and O2 [ρ (r_{bcp}) = 0.0077 au and $\nabla^2\rho$ (r_{bcp}) = 0.0283 au] and the other located between O1 and S8 with ρ (r_{bcp}) = 0.0205 and $\nabla^2\rho$ (r_{bcp}) = 0.0535 au. In addition, topological analysis confirmed one ring critical point, rcp, with ρ (r_{rcp}) = 0.0070 au and $\nabla^2\rho$ (r_{rcp}) = 0.0308 au. The relative energy for formation of the C2 complex is 0.60 kcal/mol lower than the reactant without entrancing any transition state.

The formation of C3 is the same for C2 with the same atomic connectivity just C3 is cis- CH_3O_3SH and its energy is little different from C2. Therefore, C3 is a five-membered ring structure with 0.28 kcal/mol of relative stability at the CCSD(T) level of computation without passing energy barrier. The origins of newly bonds formation are confirmed using electronic charge density and its Laplacian analysis. Base on AIM results, the O2–H4 bond with the length of 2.743 Å, has hydrogen bond character and the S8–O1 bond is defined as the van der Waals type interaction. In this complex, interaction of H4 of methanethiol with lone pair of the terminal O2 of ozone and another interaction of O1 of molecular ozone with the S8 of methanethiol occur with the O1–S8 bond length of 2.753 Å. However, the O1–S8 is shorter than the corresponding bond in C2, and the H4–O2 bond is longer than its H4–O2 bond in isolated trans-C2 molecule. The topological analyses reveal the existence of two bcp, one located between H4 and O2 with ρ (r_{bcp}) = 0.0087 au and $\nabla^2\rho$ (r_{bcp}) = 0.0315 au and another is located between O1 and S8 with ρ (r_{bcp}) = 0.0240 au and $\nabla^2\rho$ (r_{bcp}) = 0.0629 au. One rcp has been confirmed using topological analyses with ρ (r_{rcp}) = 0.0076 au and $\nabla^2\rho$ (r_{rcp}) = 0.0340 au.

In C4, interactions between two terminal oxygen atoms of ozone molecules, O1 and O3, with the sulfur atom of methanethiol are concluded a four-membered ring with 2.07 kcal/mol stability at the CCSD(T) level without entrance to any transition state. The bond length of newly formed bonds, O1–S8 and O3–S8, are 3.138 and 2.923 Å, respectively. The topological analysis reveals the presence of two bcp, one is located between O1 and S8 [ρ (r_{bcp}) = 0.0118 au and $\nabla^2\rho$ (r_{bcp}) = 0.0333 au] and the other is located between O3 and S8 [ρ (r_{bcp}) = 0.0178 au and $\nabla^2\rho$

Table 3
The total rate constant data (in cm^3 $molecule^{-1}$ s^{-1}) and its detail are calculated for P2 production at the B3LYP/6-311++G(3df,3pd) level.

Temperature	K_{eq-C1}	k_2	k_{-2}	k_3	k_T
200	1.51×10^{-25}	2.84×10^{-8}	956.029	0.035994	1.135×10^{-28}
300	1.73×10^{-25}	0.0164	3384.18	0.7917	1.217×10^{-23}
400	2.37×10^{-25}	12.896	11719.3	8.63	4.147×10^{-21}
500	3.32×10^{-25}	722.714	23999.3	37.833	1.523×10^{-19}
600	4.60×10^{-25}	10826.49	44453.1	118.912	1.863×10^{-18}
700	6.24×10^{-25}	76149.72	69739.1	272.693	1.216×10^{-17}
800	8.28×10^{-25}	333200.3	82238.1	425.517	5.334×10^{-17}
900	1.08×10^{-24}	1060,557	79095.5	505.976	1.785×10^{-16}
1000	1.37×10^{-24}	2697,748	63818.2	476.324	4.962×10^{-16}

(r_{bcp}) = 0.0461 au]. In addition, topological analysis shows one rcp with ρ (r_{rcp}) = 0.0110 au and $\nabla^2\rho$ (r_{rcp}) = 0.0415 au.

3.2. Reaction mechanism

The reaction mechanism of the bimolecular reaction between methanethiol and ozone based on initial complex can be described in different reaction pathway. First, a pre-complex is formed in all reaction pathways.

3.2.1. Reaction pathway that begins with C1

Reaction pathway that begins with C1, has been passed of the following parts and products

Path 1: $CH_3SH + O_3 \rightarrow C1 \rightarrow TS3 \rightarrow IN1 \rightarrow TS5 \rightarrow CP2 \rightarrow {}^1P2 \rightarrow {}^3P2$.

In this reaction pathway, first the hydrogen atom on the methyl group absorb by one of the terminal oxygen of ozone, and hydrogen atom on thiol group is also absorbed by others terminal oxygen of ozone molecule. C1 is directly converted to IN1 through TS3 with the energy barrier of 11.81 kcal/mol, that is to say this process is happen very easily (see Fig. 1; Table 1). TS3 has one imaginary frequency at 467i cm^{-1}, which is vibrated in the reaction coordinate. The H4–C5 bond length in TS3 is about 42% longer than that corresponding bond in C1. The H9–O1 bond length is formed in transition state TS3 that is about 5% longer than that in the IN1 molecule. Also, the transition state structure shows two hydrogen bonds that one located between H9–O1 atoms [ρ (r_{bcp}) = 0.0172 au and $\nabla^2\rho$ (r_{bcp}) = 0.0832 au] anther is shown between H4–O3 atoms with the electronic charge density of ρ (r_{bcp}) = 0.0240 au. IN1 has six-membered ring structure of CH_2S and trans-H_2O_3 that S8–H9 and O3–H6 bond lengths are 0.189 and 0.197 Å longer than those corresponding bonds in TS5. In the next step, IN1 is converted into CP2 with the passing of TS5, which trans-H_2O_3 becomes to H_2O and O_2. The energy barrier of TS5 transition state is 54.41 kcal/mol. TS5 has only one imaginary frequency of 1659i cm^{-1}. As shown in Fig. 1, transition state structure shows transfer of hydrogen atom from O3 to O1 bond, and breaks the O1–O2 bond. The O3–H4 bond length is elongated from 0.969 Å in IN1 to 1.390 Å in TS5 and the O1–H4 bond length is shortened from 1.131 Å in TS5 to 0.961 Å in H_2O molecule in CP2. The product complex CP2 can directly transform into the product ${}^1O_2({}^1\Delta_g) + CH_2S + H_2O$ through O1–O2 bond rupture without any transition state. Singlet molecular oxygen due to spin multiplicity changes and transforms to triplet oxygen through a relaxation process. The reaction thermodynamic parameters indicate that ${}^3P2$ complex, ${}^3O_2({}^3\Sigma_g) + CH_2S + H_2O$ formation is exothermic with enthalpy of reaction, −65.92 kcal/mol in comparison with the original reactants. In the all steps of path P1, the formation of products from reactants is confirmed using related IRC curves.

3.2.2. Reaction pathway that begins with C2

Reaction pathway that begins with C2 of the following parts and products that passes

Path 2: $CH_3SH + O_3 \rightarrow C2 \rightarrow TS2 \rightarrow CP1 \rightarrow {}^1P1 \rightarrow {}^3P1$.

In this reaction pathway, the oxygen atom of ozone that was oriented toward the sulfur atom in the C2, after passing of TS2 attached to sulfur atom. Eventually, lead to the production of CH_3SHO and O_2. That the way schematic is shown in Fig. 2. The energy barrier is calculated 22.15 kcal/mol at the CCSD(T) method. Imaginary frequency of TS2 is 743i cm^{-1} in the direction of reaction coordinate at B3LYP level. The optimized five-membered ring structure of TS2 transition state shows that the O9–O8 bond ruptures and formation of the O9–S5 bond. The O9–O8 bond length is 0.277 Å longer than corresponding bond in C2, and the O9–S5 bond length is 0.946 Å shorter than corresponding bond in C2. In final step, CP1 can directly be converted to ${}^1P1$ ($CH_3SHO + O_2({}^3\Sigma_g)$) via breaking of O9–O8 bond without passing through any transition state. Singlet molecular oxygen due to spin multiplicity changes and transforms to triplet oxygen through a relaxation process. The reaction thermodynamic parameters indicate that $CH_3SHO + {}^3O_2$ formation process is exothermic by −58.89 kcal/mol releasing heat and spontaneous with −57.62 kcal/mol of Gibbs free energy at atmospheric pressure and 298.15 K temperature. The formation of products along the path is confirmed using AIM results and IRC curve.

3.2.3. Reaction pathways that begins with C3

For the above initial complex, two-reaction paths obtained which are shown below:

Path 3: $CH_3SH + O_3 \rightarrow C3 \rightarrow TS8 \rightarrow IN4 \rightarrow TS10 \rightarrow IN6 \rightarrow TS12 \rightarrow IN7 \rightarrow TS14 \rightarrow CP5 \rightarrow P5$.
Path 4: $CH_3SH + O_3 \rightarrow C3 \rightarrow TS8 \rightarrow IN4 \rightarrow TS10 \rightarrow IN6 \rightarrow TS12 \rightarrow IN7 \rightarrow TS13 \rightarrow CP6 \rightarrow P6$.

Two similar pathways for production of P5 and P6 have been obtained that the ends of paths are different from each other. In the above pathways, first involves transfer of hydrogen atom of thiol group to the one of the terminal oxygen of the molecular ozone, and connecting others terminal oxygen to the sulfur atom. The mentioned processes have done with passing of TS8. Energy barrier of this transition state is 9.23 kcal/mol and imaginary frequency of TS8 is 713i cm^{-1}. The forming bond length of S8–O1 shortages from 2.753 Å in C3 to 1.118 Å in TS8 and the breaking bond length S8–H9 is 1.459 Å in TS8. In addition, another forming bond length of O3–H9 is 1.625 Å in TS8 that shortened to 0.972 Å in IN4. Then, IN4 can be exchange to IN6 through TS10 by formation of the S–O3 and breaking of the O3–O2 bonds. For this step, barrier height is 36.18 kcal/mol. The optimized structure of transition state TS10 shows the O3–O2 bond length is 15% longer than corresponding bond in IN4. Imaginary frequency of TS10 is 376i cm^{-1} in the reaction coordinate at the B3LYP level of theory. In next step, IN6 transform to IN7 through TS12 with the energy barrier of 19.49 kcal/mol at the CCSD(T) method and imaginary frequency of 492i cm^{-1} at the B3LYP level. The optimized three-membered ring structure of TS12 shows hydroxyl shift from O3 atom to S atom. The O3–O2 breaking bond length is 48% greater than corresponding bond in IN6 and the O2–S forming bond length is about 0.843 Å shorter than corresponding bond in IN7.

In path P3, the IN7 transform to CP5 after passing TS14 with 63.64 kcal/mol of the energy barrier at the CCSD(T) level. TS14 has one imaginary frequency of 1639i cm^{-1} in the direction of reaction coordinate at B3LYP level. The four-membered ring structure of TS14 is formed when the hydrogen atom of methyl group connects to oxygen atom of hydroxyl group. The O–H6 bond length in TS14 is about 24% longer than that corresponding bond in CP5. The CP5 energy is 31.40 kcal/mol lower than TS14. In the final step, CP5 can convert to product without passing of transition state. The P5, $CH_2SO_2 + H_2O$, is about −118.91 kcal/mol stable than original reactants. The reaction thermodynamic parameters show that P5 formation process is exothermic by 119.64 kcal/mol releasing heat and spontaneous with −117.99 kcal/mol of Gibbs free energy.

In path P4, the IN7 convert to CP6 through TS13 by hydroxyl group translation from sulfur atom to carbon atom. The breaking bond lengths of C–S and S–O2 is 2.423 and 1.816 Å in TS13 that and the forming bond length of C–O2 shortage from 2.105 Å in TS13 to 1.421 Å in CP6. The energy height of the process is 79.68 kcal/mol. TS13 imaginary frequency is 622i cm^{-1}. According

the topological analysis, one bcp is located between O2 of methanol and S8 of sulfur dioxide with ρ (r_{bcp}) = 0.0238 au and $\nabla^2\rho$ (r_{bcp}) = 0.0662 au. CP6 converts into P6 by rupture of O8–O2 bond without entrance any transition state. The P6 production channel has the lowest ΔH°, ΔE° and ΔG° (see Table 2) of reaction, and the formation of P6 is very exothermic and spontaneous in gas phase. Therefore, P6 is thermodynamically the main product.

3.2.4. Reaction pathways that begins with C4

For the initial complex C4, four-reaction path obtained which are shown as follows:

Path 5: $CH_3SH + O_3 \rightarrow C4 \rightarrow TS1 \rightarrow IN2 \rightarrow TS6 \rightarrow CP3 \rightarrow {}^1P3 \rightarrow {}^3P3$.
Path 6: $CH_3SH + O_3 \rightarrow C4 \rightarrow TS1 \rightarrow IN2 \rightarrow TS4 \rightarrow IN3 \rightarrow TS7 \rightarrow CP4 \rightarrow P4$.
Path 7: $CH_3SH + O_3 \rightarrow C4 \rightarrow TS9 \rightarrow IN5 \rightarrow TS11 \rightarrow IN6 \rightarrow TS12 \rightarrow IN7 \rightarrow TS14 \rightarrow CP5 \rightarrow P5$.
Path 8: $CH_3SH + O_3 \rightarrow C4 \rightarrow TS9 \rightarrow IN5 \rightarrow TS11 \rightarrow IN6 \rightarrow TS12 \rightarrow IN7 \rightarrow TS13 \rightarrow CP6 \rightarrow P6$.

In path 5, after forming the C4 from the original reactants, it can be transform into IN2 with passing of TS1. In this process, the energy height is 15.01 kcal/mol. The hydrogen interaction occurs between H5 atom of methyl group and a lone pair of oxygen atom O of molecular ozone. In addition, in the other side, non-bonding electron pairs of O1 atom in molecular ozone interact with the C4 atom of methyl group. The newly bond lengths, O3–H5 and O1–C4 in the IN2 are 0.974 and 1.406 Å, respectively. In later step, IN2 is exchange to CP3 passing through TS6 by inter-molecular interaction that involves the hydrogen atom transfer from O3 atom to O1 atom and dissociation the O1–O2 bond. In the four-membered ring structure of TS6, the O1–O2 breaking bond length is 57% greater than corresponding bond length in IN2. The length of newly bond formed is shortened about 0.652 Å in the CP3. The topological analysis of the wave function reveals the existence of two bcp, one is located between O9 of molecular oxygen and H2 atom [ρ (r_{bcp}) = 0.0187 au and $\nabla^2\rho$ (r_{bcp}) = 0.0630 au] and other is located between O9 and S atom [ρ (r_{bcp}) = 0.0224 au and $\nabla^2\rho$ (r_{bcp}) = 0.0625 au]. Results predict that the O9–H2 and O9–S bonds are van der Waals type. Also, one rcp is shown with ρ (r_{bcp}) = 0.0112 au and $\nabla^2\rho$ (r_{bcp}) = 0.0433 au. Finally, CP3 directly exchange to final product P3 by breaking of the O9–H2 and O9–S. Our results corroborate that the $CH_2SHOH + {}^3O_2$ production is exothermic (ΔH° = −79.32 kal/mol) and spontaneous (ΔG° = −78.28 kcal/mol) in gas phase at the atmospheric condition.

In path 6, the formation of IN2 is similar to path P5. Then, IN2 is transformed to IN3 after passing TS4 with the energy barrier of 86.97 kcal/mol in comparison with IN2. The five-membered ring structure of TS4 formed when O9 atom attacks to H4 atom of methylene group and same time, the O7–O5 bond is ruptured. IRC calculations indicate that during the process, dissociation of O7–O5 bond is elongated from 1.445 Å in IN2 to 2.105 Å in TS4. The imaginary frequency of TS4 is 728i cm^{-1} at B3LYP level. AIM analyses show that IN3 intermediate has a six-membered ring structure and the new bond length of O9–O4 is 0.994 Å. In addition, IN3 is 100.05 kcal/mol stable than TS4. In next step, IN3 transforms into CP4 using TS7 with 5.68 kcal/mol energy barrier at the CCSD(T) method. TS7 has one imaginary frequency at 1326i cm^{-1} that is vibrated in the reaction coordinate. In six-membered ring structure of TS7, the hydrogen atom has a bridge between two oxygen atoms, and a three-membered ring is formed between two oxygen atoms and hydrogen atom. The length of O9–H2 breaking bond is 0.381 Å longer than the corresponding bond length in IN3, which corresponds to a relative increase of 40%, and the O8–H2 bond length formed is about 10% longer than that in the isolated CP4 molecule. According the AIM analysis, CP4 has six-membered ring structure with −97.84 kcal/mol stability energy in comparison with reactants. The R → P4 exchange process is exothermic and spontaneous in gas phase with the enthalpy of reaction, ΔH° = −96.87, and free energy of reaction, ΔG° = −96.86 kcal/mol at the corresponding levels of computation.

In path 7, the C4 pre-reactive complex can be converting into IN5 after passing through TS9. In mentioned process, the ring structure of TS9 is formed when the H9 of S–H bond, interacts with a lone pair of the terminal O3 of molecular ozone, and in the other side, O1 of molecular ozone interacts with the S8 atom. The S8–O1 forming bond length is shortened from 2.177 Å in TS9 to 1.499 Å in IN5. The energy barrier of TS9 is 9.85 kcal/mol and imaginary frequency is 509i cm^{-1}. Then IN5 can become to IN6 through TS11 by breaking the O1–O2 bond and formation of S8–O2 bond. The energy barrier for done this process is 4.93 kcal/mol and imaginary frequency of TS11 is 93i cm^{-1}. Later steps of path 7 continue with IN6 formation to P5 production, which is similar to path P3 that obtained in above pathway.

In path 8, the formation of IN7 is similar to path P5 and in continues of path 8, the P6 production from IN7 is similar to path 4, which are obtained in mentioned pathways. Our results predict that the P6 formation is exothermic and spontaneous in gas phase and thermodynamically is most feasible product in comparison with others products (see Table 2).

3.3. Calculation of rate constants

Rate constant is a key parameter in the kinetic study of reaction that can be calculated from statistical mechanics. Rate constant equation is obtained from transition state theory (TST) based on statistical thermodynamics for second-order elementary reaction. Hence, we carried out rate constants calculation at the different temperatures by RRKM [31–33] and TST [33,34] theories implemented in the Ssum [35] and Gpop [36] programs.

The results reveal that the formation process of product P2 has two transition states with lower potential energy surface in comparison with the other channels. So, the favorable paths (the paths with the minimum energies) for the reaction, based on the calculations in this work, is P2 (H_2O, CH_2S and O_2). The values of the rate constants for the path P2 has been reported in Table 3 at different temperatures (200–1000 K). In this table the value of K_{eq-C1}, $K_{eq-C1} = k_1/k_{-1}$, is the equilibrium constant between the reactants and C1 where k_1 and k_{-1} are the rate constant for forward and reverse of C1 formation from reactants. The total rate constant of the C1 → TS3 → IN1 reaction and its reverse has been shown as k_2 and k_{-2} in Table 3, respectively. The rate constant for the reaction (reactant → IN1) is equal to $K_{eq-C1} * k_2$. The reaction continue with the formation of CP2 from conversion of IN1 after passing TS5 that its rate constant is shown with k_3 in table 3. RRKM theory is used to obtain the overall rate constant (k_T) of the reaction (reactant → P2) at infinite pressure, the product of the rate constants of the forward reactions should be divided to the product of the rate constant of the reverse reactions as this equation $K_{eq-C1} * k_2 * k_3/k_{-2}$. It is evident for Table 3 that the rate constant increases with the increase of temperature. Also, Thiol oxidation reactions are carried out very slow. Therefore, we discussed only the rate reaction for P2 production.

The calculated rate constants for the P2 production channel on the ground state potential energy surface at the 300 K temperature is 1.22×10^{-23} cm^3 $molecule^{-1}$ s^{-1} in atmospheric condition. The small amount of rate constant for the reaction of methanethiol with ozone indicates that this reaction in 300 K can be slow. According to data results, the rate constant of methanethiol with ozone reaction under atmospheric pressure increase with temperature, which indicates that the reaction will be accelerated in

higher temperatures. Fig. 4 is an Arrhenius curves for $CH_3SH + O_3$ reaction, where ln k_T versus 1000/T are plotted. From the ln k_T plot versus 1000/T, Arrhenius equation can be calculated as follow:

$$k_T = 6.512 \times 10^{-13}\ e^{-62.322 kJ/mol/RT}$$

4. Conclusion

From the present study, it is obvious that:

1. There are four pre-reactive complexes: C1, C2, C3 and C4, formed between methanethiol and ozone molecule. Pre-reactive complex C1 has a five-membered ring structure with a van der Waals interaction, and one hydrogen bond. The producing of C1 is barrier-less process with 1.79 kcal/mol of the stabilization energy with respect to the reactants at the CCSD(T) method. Pre-reactive complex C2, lying at 0.60 kcal/mol below the energy of original reactants, has a van der Waals interaction and one hydrogen bond. Pre-reactive complex C3, is a five-membered ring structure with 0.28 kcal/mol relative energy below the reactants. Pre-reactive complex C4, formed when terminal oxygen atoms of ozone with the sulfur atom of methanethiol are concluded a four-membered ring with 2.07 kcal/mol stability. AIM analyses show two van der Waals interaction in C4 molecule.
2. via Variety of transformations of the pre-reactive complexes and after passing transition states, six kinds of products P1 ($CH_3SHO + O_2$), P2 ($CH_2S + H_2O + O_2$), P3 ($CH_2SHOH + O_2$), P4 ($CHOSH + H_2O_2$), P5 ($CH_2SO_2 + H_2O$) and P6 ($CH_3OH + SO_2$) are obtained.
3. P6 product is the most stable product in comparison with the others. P5, P4, P3, P2 and P1 species are the other relatively stable products with negative value in Gibbs free energy. The standard entropy of reactions in different pathways are almost the same except for P2 which is extremely more than that of the other products.
4. In kinetic viewpoint, the computational results reveal that the formation process of product P2 has two transition states with the lower energy barriers in comparison other channels. So, P2 adduct is the favorable product. The rate constant values show that the production of P2 can be considerable in temperatures above 500 K. Also, thermodynamic relative stability of P2 increases with temperature due to P2 entropy production. So, at high temperatures, P2 is more important than the other adducts.

Appendix A. Supplementary material

Supplementary data associated with this article can be found, in the online version, at http://dx.doi.org/10.1016/j.comptc.2014.04.028.

References

[1] S. Bashkova, A. Bagreev, T.J. Bandosz1, Adsorption/oxidation of methyl mercaptan on activated carbons, Prepr. Pap. – Am. Chem. Soc., Div. Fuel Chem. 48 (2) (2003) 690–693.
[2] C. Limbachiya, M. Vinodkumar, M. Swadia, A. Barot, Electron impact total cross section calculation for CH_3SCH_3 (methanethiol) from threshold to 5 keV, Mol. Phys. 112 (2014) 101–106.
[3] S. Nourbakhsh, K. Norwood, H.M. Yin, C.L. Liao, C.Y. Ng, Vacuum ultraviolet photodissociation and photoionization studies of CH_3SCH_3 and CH_3S, J. Chem. Phys. 95 (1991) 5014–5023.
[4] J. Furne, J. Springfield, T. Koenig, E. DeMaster, M.D. Levitt, Oxidation of hydrogen sulfide and methanethiol to thiosulfate by rat tissues: a specialized function of the colonic mucosa 62 (2) (2001) 255–259.
[5] S. Wei-Jineg, Z. Shu-Ping, Z. Zi-Yan, Thermodynamic and kinetic investigations on the reaction of methanethiol with oxygen atom, Ind. J. Chem. 52A (2013) 1411–1415.
[6] W. Vogt, Oxidation of methionyl residues in proteins: tools, targets, and teversal, Free Radic. Biol. Med. 18 (1995) 93–105.
[7] D.A. Dickinson, H.J. Forman, Cellular glutathione and thiols metabolism, Biochem. Pharm. 64 (2002) 1019–1026.
[8] K. Capaldo, J.J. Corbett, P. Kasibhatla, P. Fischbeck, S.N. Pandis, Effects of ship emissions on sulphur cycling and radiative climate forcing over the ocean, Nature 400 (1999) 743–746.
[9] N. Eyet, S.M. Villano, V.M. Bierbaum, Anchoring the gas-phase acidity scale: from formic acid to methanethiol, Int. J. Mass Spectrom. 283 (2009) 26–29.
[10] J. Heicklen, The gas-phase oxidation of organic sulfur compounds, Rev. Chem. Int. 6 (1985) 175–196.
[11] S. Wei-Jinag, Z. Shu-Ping, Z. Zi-Yan, Thermodynamic and kinetic investigations on the reaction of methanethiol with oxygen atom, India, J. Chem 52A (2013) 1411–1415.
[12] T.S. Bates, B.K. Lamb, A. Guenther, J. Dignon, R.E. Stoiber, Sulfur emissions to the atmosphere from natural sources, J. Atmos. Chem. 14 (1992) 315–337.
[13] S. Bashkova, A. Bagreev, T.J. Bandosz1, Adsorption/oxidation of methyl mercaptan on activated carbons, Fuel Chem. Div. Prep. 47 (2) (2002) 685–686.
[14] A. Turk, E. Sakalis, J. Lessuck, H. Karamitsos, O. Rago, Ammonia injection enhances capacity of activated carbon for hydrogen sulfide and methyl mercaptan, Environ. Sci. Technol. 23 (1989) 1242–1245.
[15] G.P. Van Durme, B.F. McNamara, C.M. McGihley, Bench-scale removal of odor and volatile organic compounds at a composting facility, Water Environ. Res. 64 (1992) 19–27.
[16] R. Atkinson, R.A. Perry, Perry Jr., Rate constants for the reaction of the OH radical with CH_3SH and CH_3NH_2 over the temperature range 299–426 K, J. Chem. Phys. 66 (1977) 1578–1581.
[17] P.H. Wine, N.M. Kreutter, C.A. Gump, A.R. Ravishankara, Kinetics of hydroxyl radical reactions with the atmospheric sulfur compounds hydrogen sulfide, methanethiol, ethanethiol, and dimethyl disulfide, J. Phys. Chem. 85 (1981) 2660–2665.
[18] A.J. Hynes, P.H. Wine, Kinetics of the hydroxyl radical + methyl mercaptan reaction under atmospheric conditions, J. Phys. Chem. 91 (1987) 3672–3676.
[19] P.H. Wine, R.J. Thompson, D.H. Semmes, Kinetics of OH reactions with aliphatic thiols, Int. J. Chem. Kinet. 16 (1984) 1623–1636.
[20] I. Barnes, V. Bastian, K.H. Becker, E.H. Fink, Oxidation of sulphur compounds in the atmosphere: I. Rate constants of OH radical reactions with sulphur dioxide, hydrogen sulphide, aliphatic thiols and thiophenol, J. Atmos. Chem. 4 (1986) 445–466.
[21] A. Mellouki, A.R. Ravishankara, Does the HO_2 radical react with H_2S, CH_3SH, and CH_3SCH_3, Inter. J. Chem Kinet. 26 (1994) 355–365.
[22] T.J. Wallington, R. Atkinson, A.M. Winer, J.N. Pitts Jr., Absolute rate constants for the gas-phase reactions of the nitrogen trioxide radical with methanethiol, dimethyl sulfide, dimethyl disulfide, hydrogen sulfide, sulfur dioxide, and dimethyl ether over the temperature range 280–350 K, J. Phys. Chem. 90 (1986) 5393–5396.
[23] M.J. Frisch, G.W. Trucks, H.B. Schlegel, et al., Pople JA Gaussian 03, Revision B.03. Gaussian, Inc., Pittsburgh, PA, 2003.
[24] A.D. Becke, A new mixing of Hartree–Fock and local density-functional theories, J. Chem. Phys. 98 (1993) 1372.
[25] M.J. Frisch, J.A. Pople, J.S. Binkley, Self-consistent molecular orbital methods supplementary functions for Gaussian basis sets, J. Chem. Phys. 80 (1984) 3265–3269.
[26] G.E. Scuseria, C.L. Janssen, H.F. Schaefer, An efficient reformulation of the closed-shell coupled cluster single and double excitation (CCSD) equations, J. Chem. Phys. 89 (1988) 7382.
[27] T.J. Lee, P.R. Taylor, A diagnostic for determining the quality of single-reference electron correlation methods, Int. J. Quant. Chem. 36 (1989) 199–207.
[28] C. Gonzalez, H.B. Schlegel, An improved algorithm for reaction path following, J. Chem. Phys. 90 (1989) 2154–2161.
[29] R.G. Parr, W. Yang, Density-Functional Theory of Atoms and Molecules, Oxford University Press, Oxford, 1989.
[30] F. Biegler-Konig, J. Schoenbohm, AIM2000 2.0 EdBuro fur Innovative Software, Bielefeld, Germany 2002.
[31] P.J. Robinson, K.A. Holbrook, Unimolecular Reactions, Wiley-Inter-Science, New York, 1972.
[32] W. Forst, Theory of Unimolecular Reactions, Academic Press, New York, 1973.
[33] H. Eyring, The activated complex in chemical reactions, J. Chem. Phys. 3 (1935) 107–115.
[34] M.G. Evans, M. Polyani, Some applications of the transition state method to the calculation of reaction velocities, especially in solution, Trans. Farad. Soc. 31 (1935) 875–894.
[35] A. Miyoshi, Steady-State Unimolecular Master-Equation Solver (SSUMES), University of Tokyo, 2010.
[36] A. Miyoshi, Gaussian Post Processor (GPOP), University of Tokyo, 2010.
[37] R.D. Johnson III (ed.), NIST Computational Chemistry Comparison and Benchmark Database, NIST Standard Reference Database, Number 69. <http://cccbdb.nist.gov/>, April, 2013.
[38] P.J. Linstrom, W.G. Mallard (eds.), NIST Chemistry WebBook, NIST Standard Reference Database, National Institute of Standards and Technology, Gaithersburg, MD, Number 69. <http://webbook.nist.gov>, 2013.